Study of Valve-Integrated Microactuator Using Homogeneous Electro-Rheological Fluid

Kazuhiro Yoshida, Jung-Ho Park[1*], Hiroshi Yano[2],
Shinichi Yokota and Sonam Yun[1]

Precision and Intelligence Laboratory, Tokyo Institute of Technology,
R2-42, 4259 Nagatsuta-cho, Midori-ku, Yokohama 226-8503, Japan
[1]Advanced Industrial Technology Dept., Korea Institute of Machinery & Materials,
171 Jang-dong, Yuseong-gu, Daejeon 305-343, Korea
[2]Graduate School, Tokyo Institute of Technology,
4259 Nagatsuta-cho, Midori-ku, Yokohama 226-8503, Japan
(Currently, Mr. Yano is with Matsushita Electric Industrial Co., Ltd.)

For fluid-driven micromachines carrying out power-needing tasks such as maintenance in a limited space, a valve-integrated microactuator using a homogeneous electro-rheological (ER) fluid is proposed and developed. A valve using a homogeneous ER fluid whose viscosity is controlled by means of the applied electric field strength, termed the ER valve, consists of fixed electrodes and features a miniaturizable simple structure with high reliability. First, in this study, to realize high performance of the micro-ER valve fabricated by micromachining, the static and dynamic characteristics of the micro-ER valve with different nematic liquid crystals, bend numbers and electrode gap lengths are experimentally investigated. Second, a polyimide-diaphragm fluid microactuator whose structure is simple and without sliding parts is proposed, fabricated and tested. Third, an ER valve-integrated microactuator combining the fabricated 3-port micro-ER valve and a polyimide-diaphragm fluid microactuator is constructed with an effective size of $8.0 \times 10 \times 1.4$ mm^3 and its characteristics are experimentally examined. Finally, a microgripper driven by the ER valve-integrated microactuator is fabricated and the drive is attempted.

---

*Corresponding author, e-mail address: jhpark@kimm.re.kr

1. Introduction

With recent progress in micro-electromechanical systems (MEMS) technologies, new functional micromachines that can perform power-needing tasks in a limited space instead of human beings, such as maintenance robots for 10-mm-diameter pipes of nuclear reactors, have been investigated.[1–4] These micromachines need multiple high-power microactuators to travel in 3D space and to handle objects. An application to the above research of fluid power with a high power density in a millimeter-scale size is an attractive subject. Hence, we have been developing practical fluid-driven micromachines.[2–4] Having a flow control valve is important to control a microactuator using fluid power; however, conventional valves such as servo valves used in hydraulics and pneumatics are difficult to miniaturize because of the leaks due to the increased occurrence of large machining errors relative to the valve size. To overcome this problem, one of the authors has proposed a microvalve using electro-rheological (ER) fluids with viscosity controllability by means of an electric field, termed the micro-ER valve,[5] and its subsequent development has been performed.[6,7] We have been developing the micro-ER valve using homogeneous ER fluid,[6] which can be miniaturized using micromachining technologies and be integrated with other mechanical and electronic parts. Through experiments on its static and dynamic characteristics, the feasibility of the micro-ER valve as an advanced control component for fluid-driven micromachines was confirmed.

In this study, an ER valve-integrated microactuator is proposed and developed. First, the performance improvement and miniaturization characteristics of the micro-ER valve are experimentally investigated. Second, a polyimide-diaphragm fluid microactuator is proposed and its characteristics are experimentally investigated. Third, an ER valve-integrated microactuator is constructed using the above devices and its characteristics are experimentally investigated. Finally, a microgripper driven by the microactuator is demonstrated.

2. Micro ER Valve

2.1 *Working principle and fabrication process*

ER fluids change their viscosities in an applied electric field. ER fluids are usually classified into two types, a dispersed-particle type and a homogeneous type. The former is a suspension of polarizable particles mixed in an insulation fluid such as a silicone oil, and its yield stress can be controlled using an applied electric field, as shown in Fig. 1(a). However, it has some disadvantages of sedimentation and wear due to the particles. On the other hand, the homogeneous-type ER fluid such as liquid crystal behaves as a Newtonian fluid and its viscosity can be linearly controlled using an applied electric field, as shown in Fig. 1(b), and it can be used in micro-flow-channels because it has no dispersed particles. Furthermore, it is free from the sedimentation and wear caused by dispersed particles. Nematic liquid crystals can be used as a homogeneous ER fluid because of their large dielectric anisotropy. However, as far as we know, the mechanism of the ER effect of the homogeneous ER fluid in flow mode has not yet been clarified. We have considered that the mechanism in flow mode is as follows: The nematic liquid crystal phase is character-
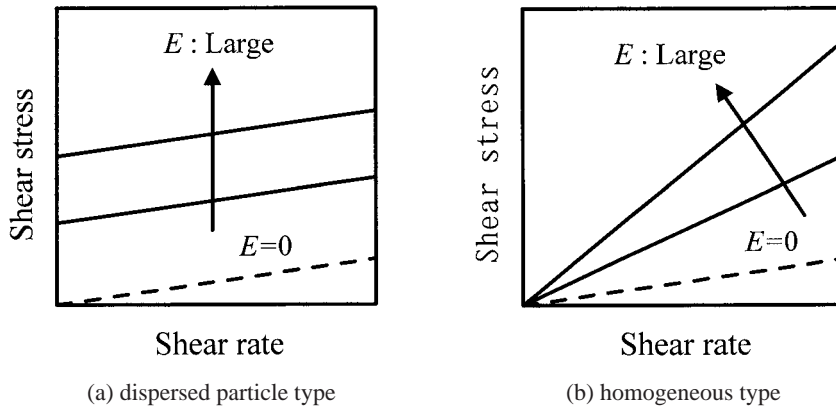
(a) dispersed particle type   (b) homogeneous type

Fig. 1.   Typical characteristics of two types of ER fluids with electric field strength *E*.

ized by rod-like molecules that tend to point in the same direction, as shown in Fig. 2(a). When an electric field is applied to the nematic liquid crystals across the parallel electrodes, the dipole molecules tend to orient themselves along the direction of the electric field, as shown in Fig. 2(b). The change in orientation of the molecules between the states shown in Figs. 2(a) and 2(b) results in a change in viscosity termed the ER effect.

The ER valve uses the homogeneous ER fluid as the working fluid and controls its flow by applying an electric field between the fixed parallel electrodes. The valve structure is simple so that it can be miniaturized and fabricated by micromachining. When electric field strength *E* is applied to the micro ER valve, the differential pressure ΔP caused by the change in viscosity at flow rate *Q* is derived as follows:

$$\Delta P = \frac{64 L_{ER}}{B_{ER} H_{ER}{}^3 \lambda} \mu(E)Q = R_{ER}(E) \cdot Q,$$ (1)

where L_{ER}, B_{ER} and H_{ER} are the length, width and gap length of the flow channel, respectively, and λ is a parameter dependent upon the channel section shape. $\mu(E)$ and $R_{ER}(E)$ are the viscosity and the channel resistance determined by the applied electric field strength *E*.

Figure 3 shows the schematic of the 2-port micro-ER valve fabricated by micromachining. The flow channel is L_{ER} = 5 mm in length, B_{ER} = 1.2 mm in width and H_{ER} = 150 μm in electrode gap length. The homogeneous ER fluid flows through a channel with a trapezoidal cross section on the silicon substrate. B_{ER} is the average width of the top and bottom sides. Figures 4(a) and 4(b) show the simplified fabrication processes. The process starts with a thermally oxidized (1μm thickness) silicon substrate (N-type, (100)) with a surface area of 20×20 mm^2 and a thickness of 200 μm. Spin-coating of positive-type photoresist (Tokyo Ohka Kogyo Co., Ltd., OFPR-800) is performed, then patterning for the alignment holes is carried out after prebaking. The silicon substrate is etched in a
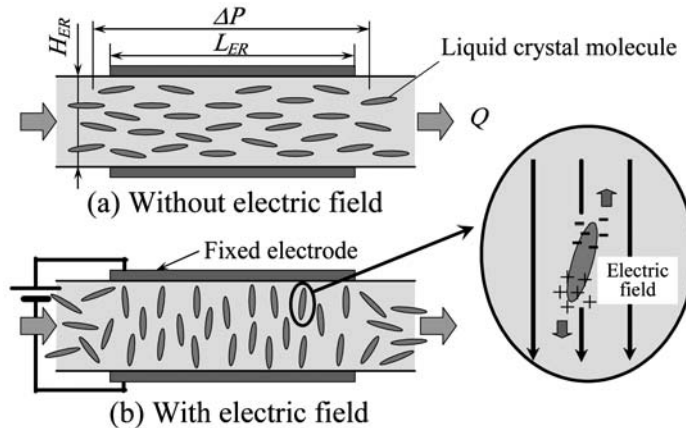
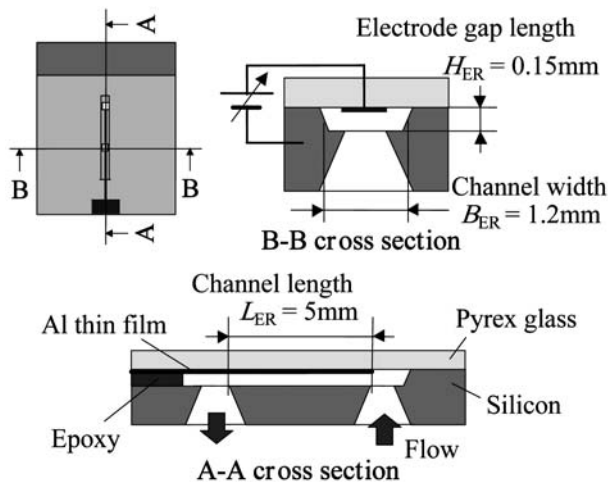Fig. 2.   Construction and working principle of 2-port valve using homogeneous ER fluid.

Fig. 3.   Schematic of 2-port micro-ER valve fabricated by micromachining.

tetramethyl ammonium hydroxide (TMAH) 15% solution after etching of the silicon dioxide layer. The patterning and TMAH etching for the inlet and outlet ports are reiterated. Then, the same process is performed on the back surface to form a flow channel and the silicon dioxide layer is completely removed. In contrast, to form the aluminum electrode, spin-coating and patterning of the photoresist on Pyrex glass are performed. The thin aluminum electrode (1 μm thickness) is then deposited by RF sputtering and lift-off is performed. Finally, the glass is anodically bonded to the silicon substrate with a voltage of 500 V at 400°C.
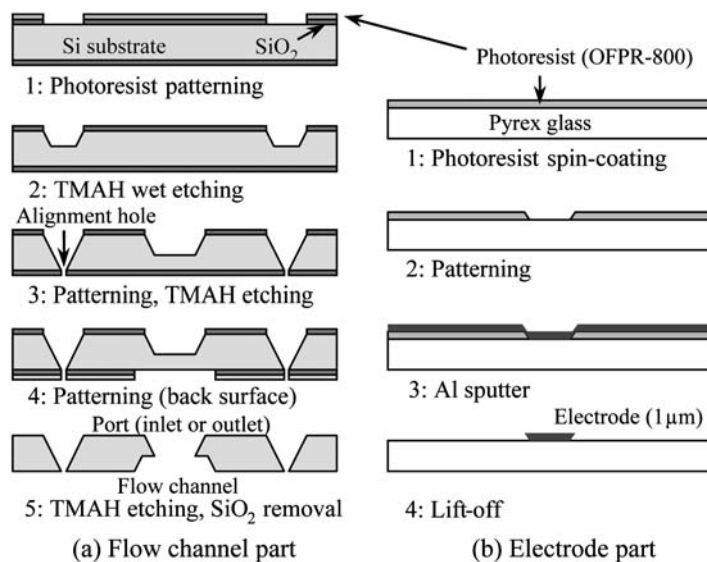
Fig. 4.   Simplified processes of 2-port micro-ER valve fabricated by micromachining.

2.2 *Selection of homogeneous ER fluid*

For fluid-driven micromachines, the base viscosity of the homogeneous ER fluid without an applied electric field is required to be as low as possible and the ER effect is required to be as high as possible. In this section, a homogeneous ER fluid suitable for fluid-driven micromachines is selected through experiments on the static and dynamic characteristics of ER fluids. On the basis of their dielectric anisotropies and base viscosities, six kinds of nematic liquid crystals are selected as the candidates: RDP-40628 (Dainippon Ink and Chemicals, Inc. This fluid was used in the previous experiments.[5]), JC-4014XX and 4015XX (Chisso Co.), and MLC-6457-000, 6425-000, and 6267-000 (Merck Japan, Ltd.).

Figure 5 shows the typical results of static characteristics between flow rate and load pressure. With increasing electric field strength, the viscosity corresponding to the slope of the graph increases. The changes in viscosity of all homogeneous ER fluids are saturated at the electric field strength of 5 kV/mm. On the basis of the experimental results, the base viscosity and the ER effect index are derived. The base viscosity μ_{min} is calculated with the slope of the approximated line of the experimental results obtained without an applied electric field. In the same way, the maximum viscosity μ_{max} with an electric field strength of 5 kV/mm is obtained and the ratio (μ_{max}/μ_{min}) is calculated as the ER effect index. Figure 6 shows the measured viscosity at different temperatures when RDP-40628 is used as a working fluid. We also investigated the influence of liquid temperature on the ER effect index and confirmed the presence of a relatively small influence.[8] The decrease in the ER effect index from 22°C to 36°C was 6.6%, but the decrease in the base viscosity was 41%. In a 3-port valve using a homogeneous ER fluid, the controllable pressure range is dominated by the ER effect index. Therefore, the variation of the base viscosity with temperature is remarkably small. The results of the three fluids with the highest perfor-
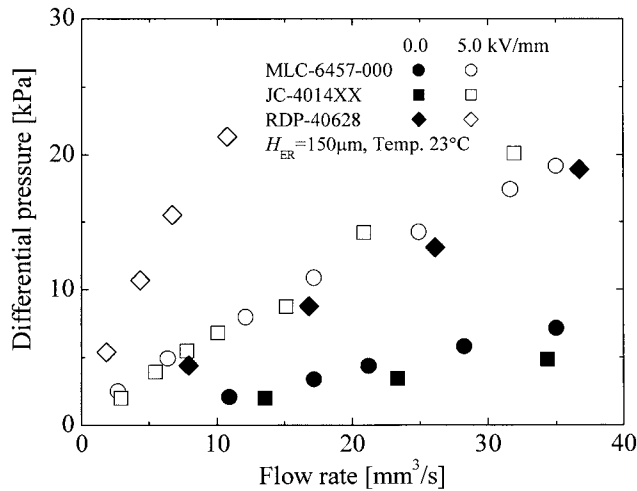
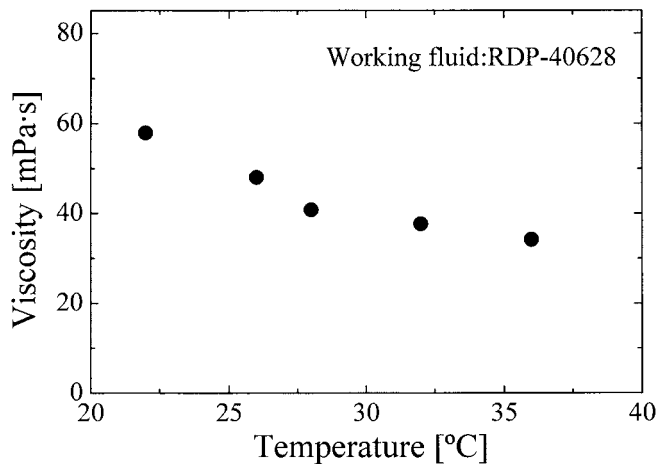Fig. 5.   Static characteristics of 2-port micro-ER valve for different homogeneous ER fluids.

Fig. 6.   Measured viscosities at different temperatures.

mances are summarized in Table 1. For the base viscosity, JC-4014XX has the lowest value and for the ER effect index, MLC-6457-000 has the highest value.

Figure 7 exemplifies the step response when MLC-6457-000 is used as the working fluid. At a constant flow rate supplied using a gear pump, the differential pressure is measured with a semiconductor-type pressure transducer (Okada Keiki Mfg. Co., Ltd., STX-20; measuring range: 200 kPa) at a sampling frequency of 375 Hz. The waveform shows 2-step responses: first, the differential pressure rapidly increases in the manner of a first-order lag response until 0.15 s, as shown in Fig. 7, then slowly increases with a slight slope. Such waveforms are considered to be caused by the increase in viscosity of nematic liquid crystals as follows: 1) nematic liquid crystal molecules are oriented very quickly,

Table 1
Comparisons of nematic liquid crystals for selection of homogeneous ER fluid suitable for micromachines.

	MLC-6457-000	JC-4014XX	RDP-40628
Density ($\times 10^3$ kg/m^3)	0.99@20°C	0.96@20°C	1.07@20°C
Dielectric anisotropy@1 kHz	10.2@20°C	7.7@25°C	27.9@25°C
Base viscosity μ_{min}(mPa·s)	24@23°C	18@23°C	60@23°C
ER effect index (μ_{max}/μ_{min})	5.4@23°C	4.6@23°C	4.2@23°C
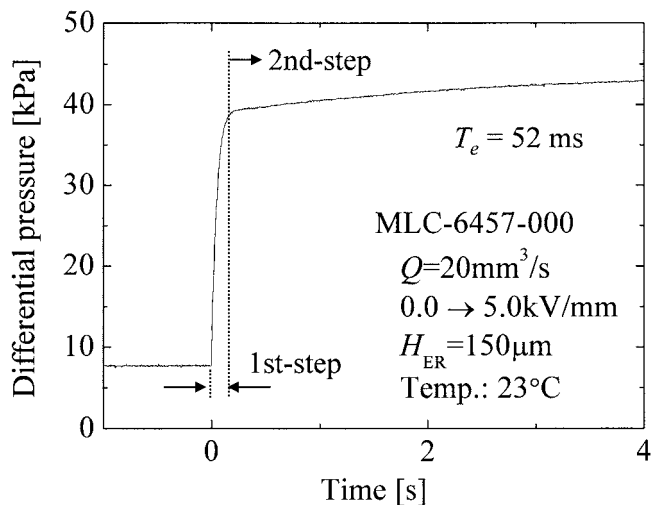
Fig. 7.   Step response of 2-port micro-ER valve at constant flow rate.

then 2) the molecule domains are concentrated slowly. In many practical applications, the flow control valves are used in feedback systems and the error is always maintained to be small. So, the first step is considered to be significant. Hence, in this study, the dynamic response is evaluated with the response index T_e in the manner of a time constant of the first-order lag responses. The response index T_e is calculated as follows: a tangent is drawn at the starting point, a point of intersection between the tangent and the horizontal line with the height of the stational value is obtained, and the time difference between the point of intersection and the starting point is obtained as the response index T_e. The calculated response index of the waveform in Fig. 7 is 52 ms.

Figure 8 shows the obtained response index for three ER fluids. The step-up responses are lower than the step-down responses for all homogeneous ER fluids. RDP-40628 has the highest response. The step responses of MLC-6457-000 and JC-4014XX are the same level for step up. The step-down responses of MLC-6457-000 are higher than those of JC-4014XX. On the basis of the experimental results, it is found that MLC-6457-000 has a low base viscosity, the highest ER effect, and medium step responses. In this study, MLC-6457-000 is selected as the homogeneous ER fluid suitable for fluid-driven micromachines.
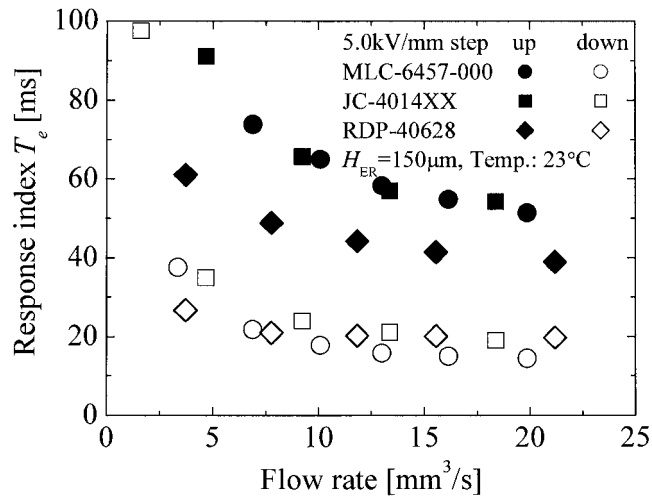
Fig. 8.   Response index T_e of 2-port micro-ER valve for different homogeneous ER fluids.

2.3 *Miniaturization characteristics of micro-ER valve*

In this section, in order to miniaturize the micro-ER valve, the characteristics of 2-port micro-ER valves with different numbers of right-angled bends and with different electrode gap lengths H_{ER} are experimentally investigated.

Figure 9 shows the top view of the evaluated flow channels of 2-port micro-ER valves. The centerlines of the flow channels have the same length of 5 mm. Figure 10 shows the experimental results of the static characteristics of the ER valves. The ER effect indices obtained are as follows: 5.1 for straight channel, 3.7 for one bend and 2.9 for two bends. Figure 11 shows the obtained response index T_e for dynamic characteristics. From these results, it is confirmed that the ER effect and the responses are degraded with the increasing number of bends. The reason is considered to be that the flow channel length is equiva-lently reduced as the flow at the bends is biased. The design of the shape and size of the bends for miniaturization of the micro-ER valve requires more consideration.

The static characteristics have been clarified to be independent of the electrode gap length.[6] In this study, the step responses are experimentally investigated. Figure 12 shows the experimental results. The flow rate is normalized using the flow channel size. It is found that the response with the electrode gap length $H_{ER} = 80$ μm is low. When the applied voltage reduction is also taken into consideration, $H_{ER} = 110$ μm is desirable.

3   Polyimide-Diaphragm Fluid Microactuator

3.1 *Proposition and fabrication*

As a compact fluid microactuator, a polyimide-diaphragm fluid microactuator, as shown in Fig. 13, is proposed, fabricated and tested. Compared with several materials that can be easily processed by micromachining, it was ascertained that polyimide is flexible and has high strength. The polyimide diaphragm is deflected by the internal pressure and the deflection is utilized as the output displacement. The structure is simple and has no
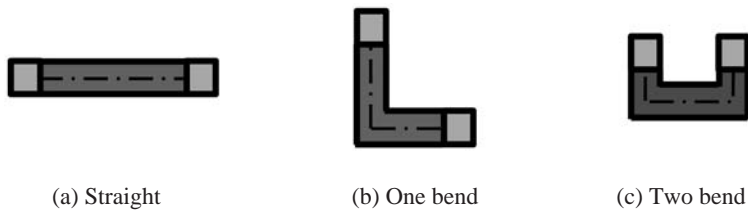
(a) Straight   (b) One bend   (c) Two bend

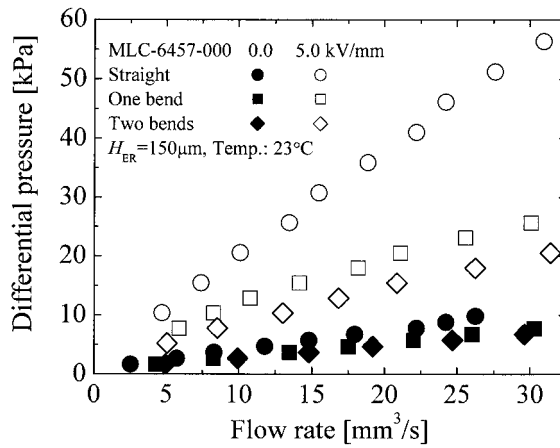Fig. 9.   Shapes of flow channels.

Fig. 10.   Static characteristics of 2-port micro-ER valve for different flow channels.
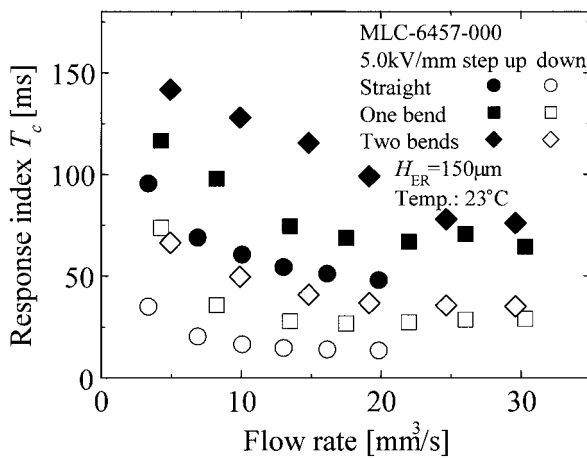

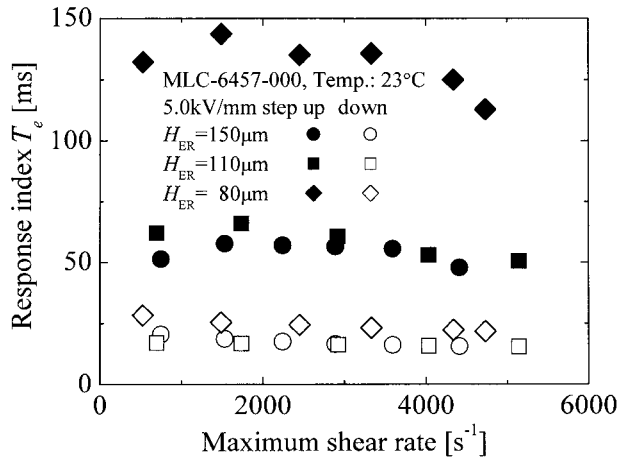Fig. 11.   Response index T_e of 2-port micro-ER valve for different flow channels.

Fig. 12.   Response index T_e of 2-port micro-ER valve for different electrode gap lengths.
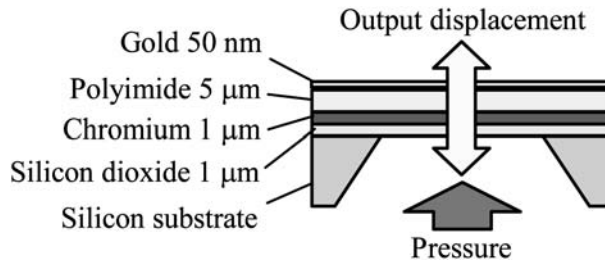

Fig. 13.   Schematic of polyimide-diaphragm fluid microactuator.

sliding parts. Hence, it is easy to fabricate by micromachining without leak problems and can be integrated with the other mechanical parts such as the micro-ER valve.

The fabricated diaphragm is composed of polyimide, chromium, and silicon dioxide layers, as shown in Fig. 13. The substrate is a silicon wafer with a silicon dioxide layer of 200 µm thickness on both sides. First, patterning is performed on the silicon dioxide layer and the substrate is anisotropically etched in TMAH 15% solution until the depth becomes half of the wafer thickness. Chromium is sputtered on the back surface to 1 µm thickness to protect the silicon dioxide layer when polyimide is spin-coated. Next, silicon etching is performed until the silicon substrate is passed through. Then, polyimide (Toray Industries Inc., SP-341) is spin-coated and baked. The polyimide thickness is 5 µm. Finally, gold is sputtered to 50 nm thickness as the target for a laser displacement meter.

3.2   *Experiments*

Even with the same fabrication process, some diaphragms are uneven while others are even. The reason is considered to be the residual stress from when the chromium layer is formed. In the experiments, the effect of flatness on the static characteristics is investigated.

In the experiments, the internal pressure and the output displacement are measured using a semiconductor-type pressure transducer (Okada Keiki Mfg. Co., Ltd., STX-20; measuring range: 200 kPa) and a laser displacement meter (Keyence Co., LC-2400; measuring range: ±3 mm, resolution: 0.2 μm). The origin of the output displacement is on the substrate surface. Figure 14 shows the experimental results for the case of a 4×4 mm^2 diaphragm size. It is found that the static characteristics of the even diaphragm have a higher linearity over a wide range and that the maximum displacement of the uneven diaphragm is larger than that of the even diaphragm. We consider that the even diaphragm is suitable for servo control systems and the uneven one is suitable for on/off motion control systems.

The static characteristics of microactuators with different diaphragm sizes are experimentally investigated. As it is difficult to fabricate an even diaphragm with a large size, all the evaluated diaphragms are uneven. The static characteristics between the pressure applied by the head and the output displacement are shown in Fig. 15. It is found that all microactuators have the same linear range and that the stepwise displacement change is large for those of a large size. The measured fracture pressures of the microactuators are 85 kPa for the 4×4 mm^2 size, 40 kPa for the 5×5 mm^2 size, and 30 kPa for the 6×6 mm^2 size with the same thickness.

4.   ER Valve-Integrated Microactuator

4.1 *Proposition and fabrication*

Each fluid microactuator requires a microvalve to control it. For compactness, in this study, an ER valve-integrated microactuator is proposed. The fabricated 3-port micro-ER valve and the polyimide-diaphragm fluid microactuator are combined and the ER valve-integrated microactuator is constructed. As shown in Fig. 16, the 3-port micro-ER valve that is used to drive the microactuator is composed of two 2-port micro-ER valves
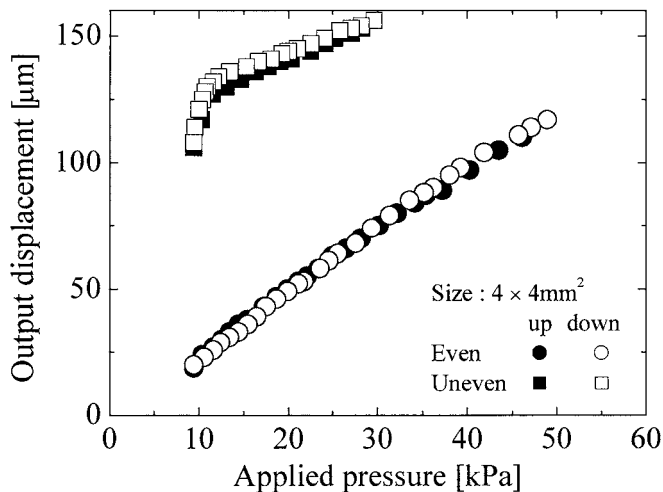

Fig. 14.   Static characteristics between pressure and displacement of polyimide-diaphragm fluid microactuator.
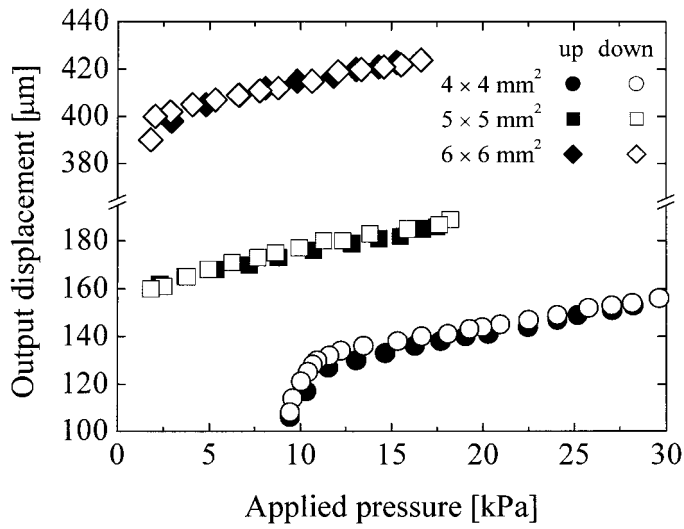
Fig. 15.   Static characteristics of polyimide-diaphragm fluid microactuator with different diaphragm sizes.
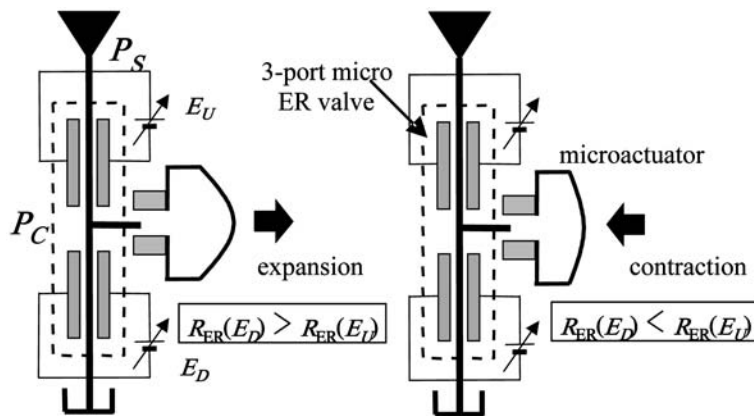

Fig. 16.   Configuration and control method for ER valve-integrated microactuator.

connected in series. The control pressure P_C with supply pressure P_S and no load flow rate is derived based on eq. (1) as follows:

$$P_C = \frac{R_{ER}(E_d)}{R_{ER}(E_u) + R_{ER}(E_d)} P_S,$$

(2)

where E_u and E_d are the electric field strengths for the upstream and downstream electrodes.

If the ER effect index in a 2-port ER valve is 3, then the controllable load pressure is from 25% to 75% of the supply pressure.

Figure 17 shows the schematics of the fabricated microactuator. The size is $8.0 \times 10 \times 1.4$ mm^3. Each of the upstream and downstream flow channels with electrodes has the same shape as the 2-port micro-ER valve of $L_{ER} = 5$ mm in length, $B_{ER} = 1.2$ mm in width, and $H_{ER} = 150$ µm in electrode gap length. In the fabricated microactuator, the electrode gap length is set to be $H_{ER} = 150$ µm for easy treatment of the residual bubbles. The structure has two parts. One part that consists of one of the silicon substrates and Pyrex glass connected by anodic bonding is for the micro-ER valve, and the other silicon substrate is for the fluid microactuator. The two parts are connected by adhesive. The flow supplied with an outside fluid power source is controlled using the 3-port micro-ER valve and applied to the polyimide-diaphragm fluid microactuator.

4.2 *Experiments*

Static characteristics are measured for different supply pressures. In the experiments, the diaphragm size is 4×4 mm^2 and MLC-6457-000 is used as the working fluid. From the experimental results, as shown in Fig. 18, it is confirmed that the pressure control range is 24 to 86% of the supply pressure of 95 kPa. The output displacement range is 40 µm. The hysteresis is large at high pressure. It will be reduced with an even diaphragm.

Figure 19 shows the step responses of the ER valve-integrated microactuator. The applied electric field strengths E_u and E_d for the upstream electrodes from supply port to control port and the downstream electrodes from control port to drain port, respectively (as shown in Fig. 17), have square waveforms at a frequency of 0.02 Hz and a sum of 5.0 kV/mm, which is a constant. As the flow occurs, the response is degraded. The rise times of control pressures are 1.3 s for step up and 0.58 s for step down. The rise times for the output displacements are 2.3 s for step up and 2.2 s for step down.
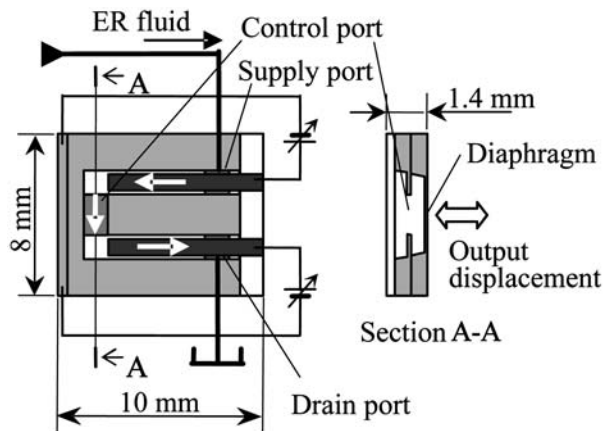

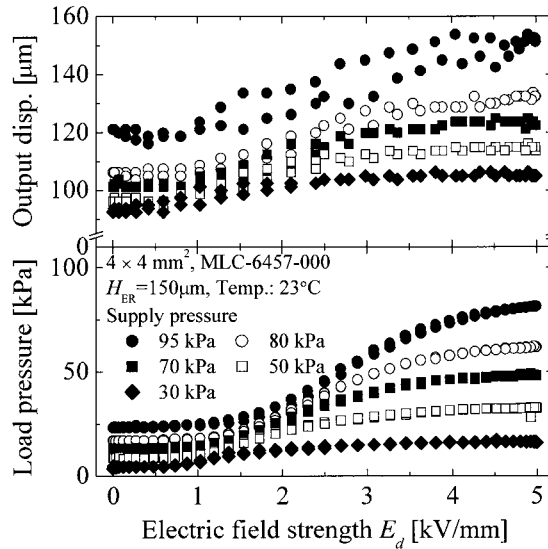Fig. 17.   Schematics of fabricated ER valve-integrated microactuator.

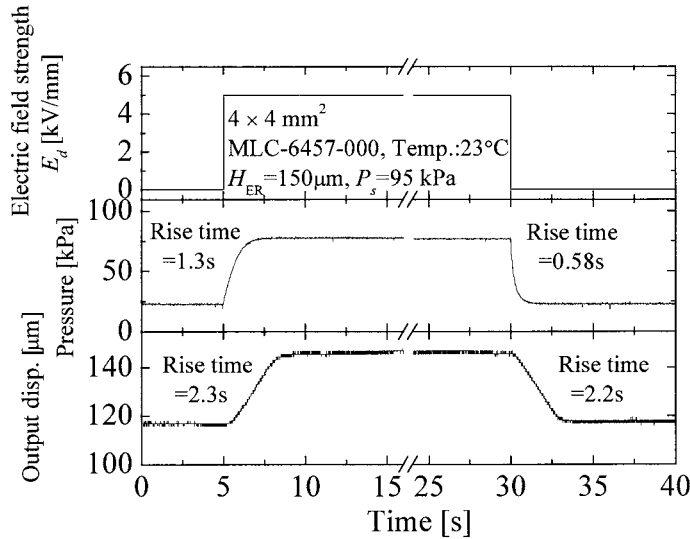Fig. 18. Static characteristics of ER valve-integrated microactuator for different supply pressures.

Fig. 19.   Step responses of ER valve-integrated microactuator.

4.3 *Application to microgripper*

As a practical application for fluid-driven micromachines, a microgripper driven by the ER valve-integrated microactuator is fabricated and the drive is attempted. Figure 20 shows the schematic of the fabricated microgripper. The finger is supported by an elastic hinge and is driven by the ER valve-integrated microactuator through a threefold lever mechanism. The size of the employed diaphragm is 6×6 mm^2.

Figure 21 shows the measured static characteristics of the microgripper for different supply pressures. Although the obtained value is smaller than the designed value, the tip displacement of 80 µm is confirmed with a supply pressure of 40 kPa.
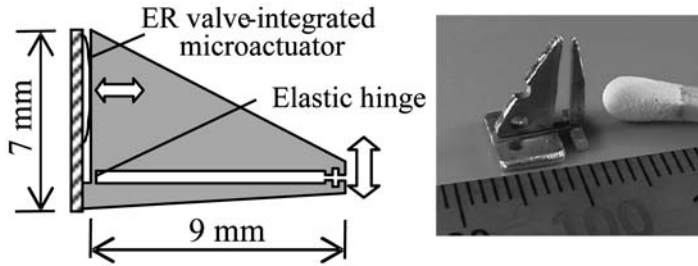
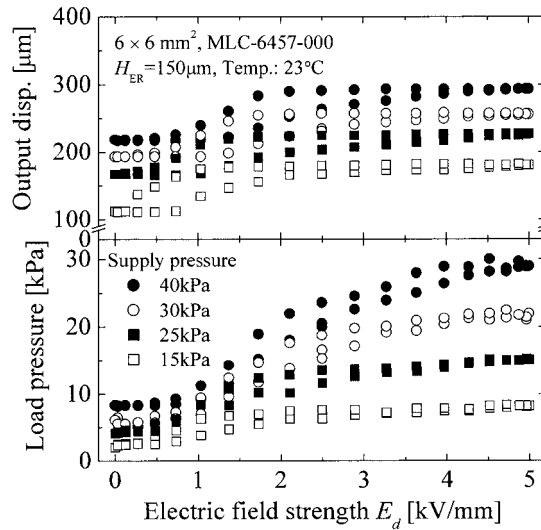Fig. 20.   Schematics of microgripper driven using ER valve-integrated microactuator.

Fig. 21.   Static characteristics of microgripper driven using ER valve-integrated microactuator.

5.   Conclusions

In this study, to realize a compact microactuator for practical fluid-driven micromachines, an ER valve-integrated fluid microactuator was proposed, fabricated and tested with the following results:
(1) To attain high performance of the micro-ER valve, MLC-6457-000 was selected as a homogeneous ER fluid suitable for micromachines on the basis of its static and dynamic characteristics. (2) To miniaturize the micro-ER valve, the static and dynamic characteristics of micro-ER valves with different bend numbers and electrode gap lengths were experimentally clarified. (3) A polyimide-diaphragm fluid microactuator was proposed and fabricated. The characteristics were clarified through experiments. (4) An ER valve-integrated microactuator was proposed and fabricated with an effective size of 8.0×10×1.4 mm^3. Its characteristics were experimentally clarified. (5) As an application of the proposed microactuator, a microgripper was fabricated and the drive was attempted.

References

1   M. Takeda: Proc. of the MEMS 2001 (2001) p. 182.
2   K. Yoshida, K. Takahashi and S. Yokota: JSME International Journal B **43** (2000) 29.
3   K. Yoshida, J. -H. Park, T. Shimizu and S. Yokota: Proc. of the 3rd IFToMM International Micromechanisms Symposium (2001) 2.
4   K. Yoshida and S. Yokota: Proc. of the FLOMEKO'93 **1** (1993) p. 122.
5   Y. Kondoh and S. Yokota: Proc. of the IROS'97 **3** (1997) p. 1672.
6   K. Yoshida, M. Kikuchi, J. -H. Park and S. Yokota: Sensors and Actuators A **95** (2002) 227.
7   M. Kohl: Mechatronics **10** (2000) 583.
8   J. -H. Park, K. Yoshida and S. Yokota: Proc. of the IROS'99 **2** (1999) p. 1063.